Characterizing spacecraft potential effects on measured particle trajectories

A. C. Barrie, F. Cipriani, C. P. Escoubet, S. Toledo-Redondo, R. Nakamura, K. Torkar, Z. Sternovsky, S. Elkington, D. Gershman, B. Giles, et al.

Physics of Plasmas

Characterizing spacecraft potential effects on measured particle trajectories

Cite as: Phys. Plasmas **26**, 103504 (2019); https://doi.org/10.1063/1.5119344
Submitted: 10 July 2019 • Accepted: 06 September 2019 • Published Online: 09 October 2019

A. C. Barrie, F. Cipriani, C. P. Escoubet, et al.

Physics of Plasmas ARTICLE scitation.org/journal/php

Characterizing spacecraft potential effects on measured particle trajectories

Cite as: Phys. Plasmas **26**, 103504 (2019); doi: 10.1063/1.5119344
Submitted: 10 July 2019 · Accepted: 6 September 2019 ·
Published Online: 9 October 2019

A. C. Barrie,[1,2] F. Cipriani,[3] C. P. Escoubet,[4] S. Toledo-Redondo,[5] R. Nakamura,[6] K. Torkar,[6] Z. Sternovsky,[7,8] S. Elkington,[8,9] D. Gershman,[2] B. Giles,[2] and C. Schiff[2]

AFFILIATIONS

[1]Aurora Engineering, Orono, Maine 04473, USA
[2]NASA Goddard Space Flight Center, Greenbelt, Maryland 20771, USA
[3]European Space Agency, Paris, France
[4]ESA/ESTEC, Noordwijk, The Netherlands
[5]Institut de Recherche en Astrophysique et Planétologie, Université de Toulouse, CNRS, UPS, CNES, Toulouse, France
[6]Space Research Institute, Austrian Academy of Sciences, Graz, Austria
[7]Smead Aerospace Engineering Sciences Department, University of Colorado, Boulder, Colorado 80309, USA
[8]Laboratory for Atmospheric and Space Physics, Aerospace Engineering Sciences Department, University of Colorado, Boulder, Colorado 80309, USA
[9]Physics Department, University of Colorado, Boulder, Colorado 80309, USA

ABSTRACT

As spacecraft does not have an independent method to conduct charge to ground, it naturally accumulates charge due to interactions with the ambient plasma and surface emission. This charge produces an electric field surrounding the spacecraft, which takes the form of a plasma sheath. Charged particles traveling through this sheath are altered in both energy and direction, thus affecting derived scientific quantities. While this effect has been known since the advent of space based particle instruments, this work represents the first time that an *in situ* characterization study of this effect has been possible. The Fast Plasma Investigation, of the Magnetospheric Multiscale mission, obtains near simultaneous measurements of phase space, via particle counts from 512 look directions and 32 energies. These new data allow the relative effects of the plasma sheath to be explored at a high time and spatial resolution. This work presents a method by which these measurements are used to study a ground model that traces the migration of particles through the sheath and estimates the error in measured velocity. This approach, performed statistically, leads to an estimation of uncertainty in particle count distributions for a given location in phase space and characterization of the redistribution of counts within a skymap due to sheath effects.

I. INTRODUCTION

The Fast Plasma Investigation (FPI) is a suite of particle detection instruments on board the Magnetospheric Multiscale (MMS) mission.[1,2] MMS consists of four identical spacecraft looking for signatures of magnetic reconnection in the magnetotail and at the day side magnetopause. On each spacecraft, FPI measures particles using four Dual Electron Spectrometers (DESs) and four Dual Ion Spectrometers (DISs). The units are placed 90° apart on the spacecraft and each has a 90° field of view in azimuth, allowing for a full 360° view among the four together. Each dual unit consists of two top hat spectrometers,[3] with each spectrometer measuring four electrostatic deflection states in azimuth and using a segmented anode to measure 16 simultaneous elevation angles, covering a full 180°.

As particles approach the MMS spacecraft, they are affected by the potential of the spacecraft that is acquired by charging in the local plasma environment.[4–6] The resulting electric field alters the trajectories of the particles affecting both the direction and energy. FPI, similar to previous missions, corrects for the energy by adjusting the measured energy by the spacecraft potential.[7,8] This correction assumes a spacecraft potential profile with spherical symmetry, and the directional error is not currently accounted for by plasma counting instrumentation suites.

There are several factors that make the nonspherical case hard to characterize:

1. The sensors are not in the same physical location on the spacecraft, but are spaced on the perimeter, 90° apart, and are thus exposed to different environments, owing to differences in sun exposure, orientation relative to the local magnetic field, directional plasma flows, etc.
2. In addition to ambient plasma, there is an Active SPacecraft POtential Control (ASPOC) system that emits a plume of positively charged indium ions into a highly localized area of the sheath.[9] The Electron Drift Instrument (EDI) also emits charged particles (electrons), affecting the sheath environment.[10,11] Similarly, there are low energy photoelectrons and secondary electrons emitted from the spacecraft surface.[12,13]
3. MMS has eight long booms that measure magnetic and electric fields. These booms will also have a charge on them, which affects the sheath in a local area near the booms.[1,11,14]
4. FPI measures electrons down to 6 eV and ions down to 2 eV, where a spacecraft charge of several volts can have a profound effect on the particle trajectory.[2,15]

These factors lead to a local electric field around the spacecraft that is nonintuitive and changes with time and location, and thus, modeling it numerically is computationally expensive. In the past, some work has been done on analytical models for simplified spacecraft in stationary environments,[4–6,15] and limited work has been done on modeling sheath effects computationally.[13,16–19] Experimentation has also been performed in ground tests to measure spacecraft sheath properties.[20,21] It has thus far not been possible, however, to accurately model for the sheath effect on particle trajectories in an operational environment or to validate simulation/experimental results with operational flight data.

One of the primary reasons why an operational model was not possible is due to the resolution of the measurements themselves. Previous missions have typically integrated counts over the course of a spin with either one or two detectors.[22–24] In this type of setup, there are only ever one or two directions of measurement in the spacecraft frame, around the axis of spacecraft spin. This makes it impossible to resolve the spacecraft sheath in flight, which in turn makes it impossible to validate or tune any simulated model.

In contrast, FPI has eight spectrometers of each species, each with four azimuthal electrostatic look directions, generating 32 independent measurement directions around the spacecraft spin axis (the spin rate is ∼3 Hz). Each azimuthal position is paired with 16 elevation look directions, for a total of 512 independent measurement directions per species, repeated at 32 different energies, all taken within 32/ms for electrons and 150 ms for ions, about 100 times faster than previous missions.[2,23,24] These advancements allow different look directions to be compared with each other, as they pass through the same environment, to map out which look directions, from the spacecraft reference frame, over or under count particles. This bias map represents an ideal metric by which a model of the spacecraft plasma sheath can be characterized and validated.

This work introduces a method whereby a detection efficiency map is created with flight data, which conveys a relative detection bias for every look angle/energy combination. This map is then reproduced via a ground simulation of particle traces through the spacecraft potential sheath. Once validated with flight data, the simulation can then be used to determine how individual particles migrated from their initial position in phase space to their final point of detection. A final characterization study of the effects of the plasma sheath on the measured particles is then presented via a map of uncertainty and a gradient map of particle migration.

II. OBSERVED FEATURES IN FLIGHT DATA

When looking closely at the raw, uncorrected data, of the highest time resolution science mode, systematic artifacts are shown in the count rates. Figure 1 shows sample data from MMS1 from August 2016. These six images are efficiency maps, each showing normalized electron count rates for the lowest energy bin (∼10–13 eV), where effects are the most pronounced. Red areas imply overcounting, and blue areas imply undercounting. The plots are in a spacecraft fixed reference frame, meaning that features of the image that are fixed in time can be isolated to a spacecraft location. These snapshots are representative of thousands of intervals examined from August of 2016, totaling over a million individual skymaps. They illustrate that, while there is some variability from interval to interval, the overall structure of this bias is consistent. Because the bias shapes are invariant with time, it can be inferred that this effect is not environmental, but rather a systematic bias introduced by the spacecraft.

The six images from different days show elevated count rates (red areas) along the top and bottom of the image, as well as several vertical bands of the elevated count rate. Figure 2 shows similar plots for all four observatories, showing agreement over much of the map area. Because all four observatories show a similar structure, subtle changes in individual spectrometers' efficiency can also be ruled out as the underlying cause for these biases. Rather, these features are artifacts introduced by the spacecraft geometry (discussed in more detail in Sec. IV.) Specifically,

1. The green rectangles show ragged bands of high count bias along the top and bottom of the image. These pixels are all looking within 11.25° of vertical with respect to the spin axis, roughly along the axial double probe (ADP).[25]
2. The purple squares represent 2 × 2 groupings that lie every 90° along the look direction of the spin plane double probes (SDPs).[14]
3. The yellow rectangles are also offset by 90° and occur at the azimuthal location of the SDP, but over a wider elevation band.

There are also several features that are not consistent between the observatories, annotated with gray + signs. It was confirmed that the gray arrow identified regions, which differ between observatories, are still self-consistent in time and are stationary in the spacecraft frame over the time period examined (August 2016). What the consistency in time suggests is that features of the spacecraft itself alter the trajectories of the measured particles through the ambient electric field. These features, which are not consistent across the four spacecraft, may be evidence of detection efficiency variations in the units, or, in some cases, related to the ASPOC plumes, which may not be identical between the emitters.[9] The expected ASPOC plume locations are annotated with gray arrows. This represents for the first time that the angular resolution of a plasma measurement suite was sufficient to obtain a map of the true biasing effect of the spacecraft plasma sheath.

Because these effects are more pronounced at the lowest energies, they do not have a large effect on integrated plasma moments and can often be ignored for studies of bulk plasma parameters, particularly for

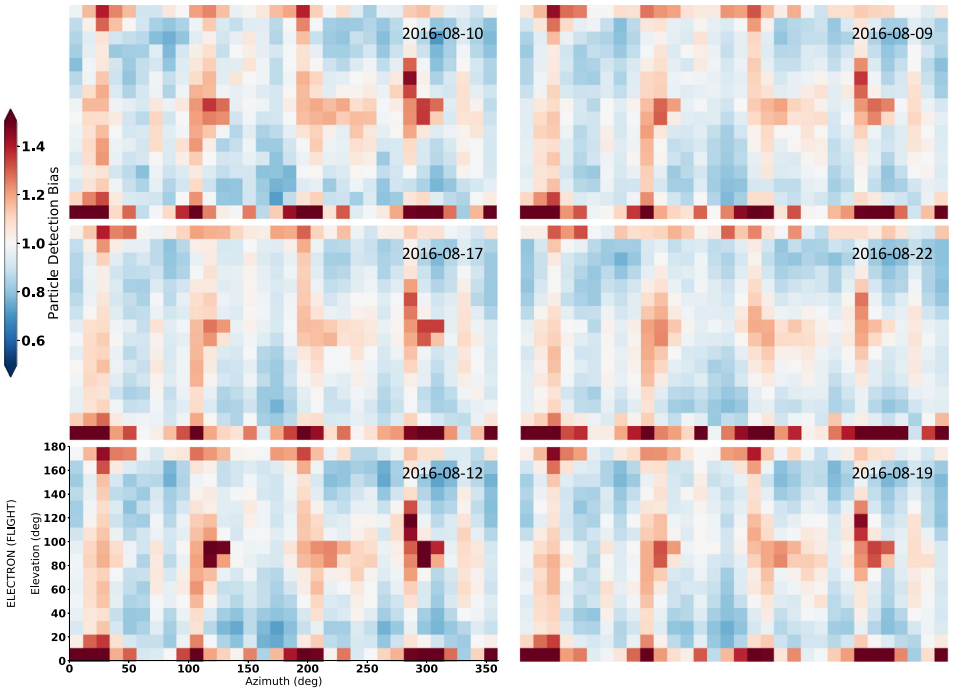

FIG. 1. Flight electron (DES) bias maps from six selected regions from August, 2016, from MMS1, at the lowest energy bin (∼10–13 eV). Data from several seconds are summed to improve statistical significance. Regions from each spectrometer are independently normalized. All maps show a similar qualitative shape with minor differences. In the absence of sheath effects, all biases would be expected to be within ∼5% of 1.00, owing primarily to the variation in instrument efficiency.[2]

higher energy plasmas. One exception to this is that subtle periodic signatures can be introduced in the integrated plasma moments.[26]

For low energy studies, particularly those involving cold beams, however, this effect can be impactful on science objectives. The signal can be lost entirely due to sheath effects,[27] as shown in Sec. IV. While this study is focused on FPI, this effect is universal to all space instrumentation which measures charged particles, including other sensors on MMS. Of the sensors on MMS,

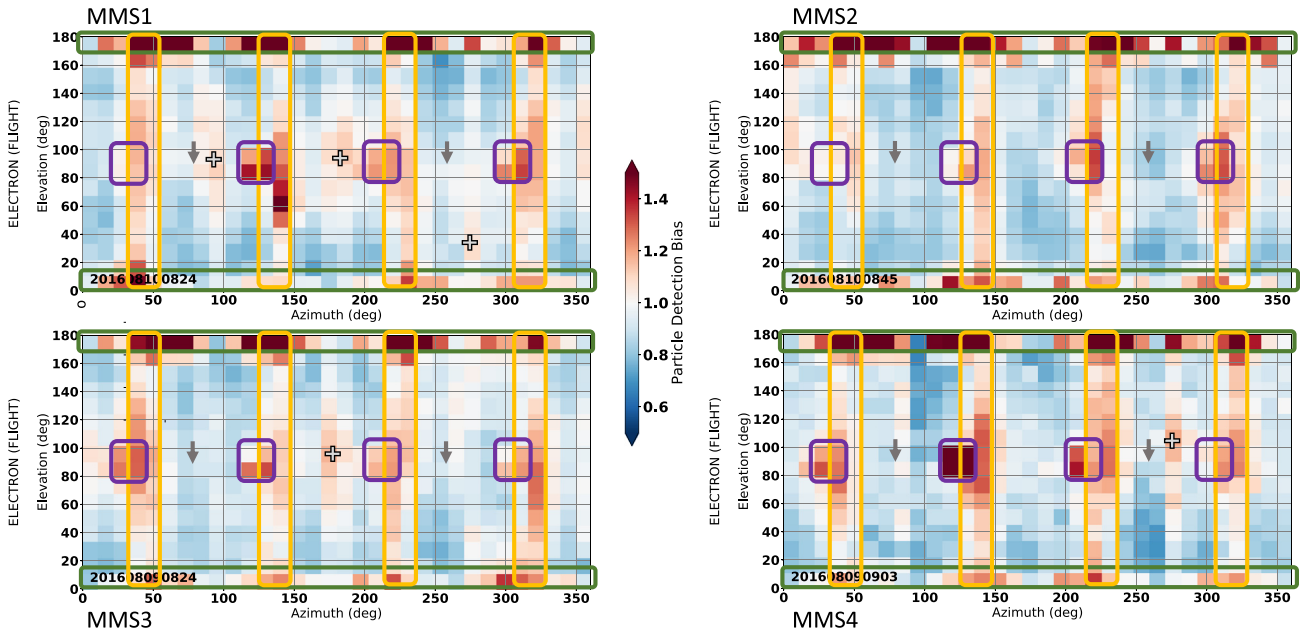

FIG. 2. Flight electron (DES) bias maps (∼10–13 eV) for all four observatories in similar environments. Data from several seconds are summed to improve statistical significance. Colored rectangles show areas of qualitative agreement, and gray + signs show areas of discrepency between the observatories. Gray arrows show the expected locations of the ASPOC emission plumes.

TABLE I. Plasma parameters used for SPIS charging simulation. Values are approximations of MMS values from 2016-08-14, 08:00 UTC. Two runs were performed, one with ASPOC emitting in a nominal fashion and the other with the ASPOC plumes not modeled. For the ASPOC-off case, the spacecraft potential was fixed to the value obtained by the ASPOC-on case.

Parameter	Value
Number density	0.5/cc
Electron temperature	500 eV
Ion temperature	3500 eV
Electron drift velocity	0 km/s
Ion drift velocity	25 km/s
Spacecraft potential	4.6 V

however, FPI operates at the lowest energy and is therefore affected the most.

III. SIMULATIONS IN THE MAGNETOTAIL

While the flight data can illustrate relative biases for particle counting (Figs. 1 and 2), it is not clear from these data alone, the magnitude to which a given particle is affected. A simulation of particle paths through the plasma sheath was undertaken to answer this question, using the high resolution flight data as a validation of the approach. The model was divided into two phases: a model of the spacecraft plasma sheath and an analysis of particle trajectories through the sheath.

Spacecraft tends to charge to a positive potential, when sunlit, due to the emission of photoelectrons. This potential will decay over some distance, based on the ambient plasma environment and the current balance at the spacecraft surface.[28,29] Based on the ambient plasma conditions used in the model (Table I), the electron Debye length scale, λ_D, is on the order of a few hundred meters,

$$\lambda_D = \sqrt{\epsilon_0 K_B T_e / n_e q^2} \simeq 235\,\mathrm{m}, \tag{1}$$

where ϵ_0 is the vacuum dielectric permittivity, K_B is the Boltzmann constant, and q is the electron charge. While the Debye scale can be useful in a first order estimate of a plasma sheath thickness away from a surface, the reality is often more complicated due to local effects.[29] Specifically, surface emission, ASPOC[9] and EDI[10] emitter plumes, complex geometrical features, an evolving local environment, etc., all alter the shape of the plasma sheath surrounding the spacecraft. As such, an analytical solution is not possible, and a numerical simulation is required to accurately resolve the sheath around the spacecraft.

The interaction of the MMS platform with its plasma environment was modeled to study the effects of the emitted ASPOC plume on the ambient environment and on the spacecraft charge state.[30,31] The results of that study were used as initial inputs here, with permission. SPIS v5.1.8[32] was used for the initial simulation of the spacecraft potential and plasma sheath. SPIS uses a Newton type solver to approximate the spacecraft geometry as an electric circuit, while using a combination of Particle in Cell (PIC) and several builtin distribution functions to solve for space charge. The multiphysics approach allows the ambient environment to iteratively inform the charge state of the spacecraft, and vice versa, until a steady state is reached. The spacecraft geometry was simplified to include all spacecraft surface elements including the Spin-plane Double Probes (SDPs)[14] and the Axial Double Probes (ADPs),[25] as well as the ASPOC system, but not the fine details of the model, such as fasteners. In this model, the ambient space potential and spacecraft potential are self-consistently solved accounting for the ambient plasma population densities and temperatures, as well as photoelectrons from solar UV, secondary electrons from higher energy particle impacts, and ASPOC beam ions, for given illumination conditions and ASPOC operating currents. The specific conditions chosen for this simulation, shown in Table I, were based on the ambient MMS environment from 2016–08-14 at ∼08:00 UTC. Separate simulations were run, first with ASPOC plumes included and second with the ASPOC plumes removed, but with the spacecraft potential fixed at the value obtained from the ASPOC-on case.

The resulting potential map from the SPIS simulation with the ASPOC plumes not included is shown in Fig. 3 (the ASPOC-on case is not included here as it is not referenced often in the ensuing work). A diagram of the MMS spacecraft is overlaid on the figure to provide context and annotate the locations of the FPI sensors. The provided azimuth reference is maintained throughout this work. Both the 60 m SDP wire booms and the 17 m ADP lattice boom have similar voltages to the main spacecraft body, at ∼4.6 V. The results are consistent with expectations in that:

- The potential is uniform over the surface of the spacecraft, which is consistent with ground testing and mission requirements mandating not more than 1 V potential across any two surface points.

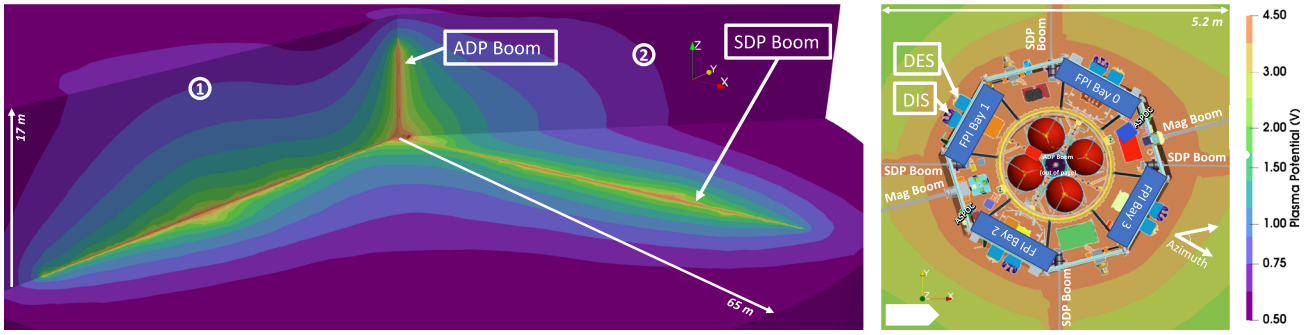

FIG. 3. Ambient potential as calculated by the SPIS model. The left panel shows an orthographic cutout. The right panel shows a zoom in of the area near the spacecraft, with the MMS spacecraft overlaid showing instrument locations. Annotations show the boom locations as well as the FPI sensor locations. Note that similar DES/DIS pairs are in all four of the annotated FPI bays. The azimuth angle for all future figures is as annotated here as is the direction of the Sun.

- The potential of 4.6 V is consistent with flight measurements for the stated operating conditions.
- As discussed in Sec. IV, this sheath solution yields counting biases consistent with measured flight data.

The potential takes several meters to taper off. Of particular note is that there is an appreciable potential, over 1 V, 10 m above the SDP boom (position 1). By contrast, the potential 45° offset from the SDP at a similar height shows a much lower potential (position 2). The sun direction is noted to emphasize that, in order to reach a steady state solution in the simulation, the sun direction was static, and so photoelectron emission does not migrate around the spacecraft as would be the case in flight. This assumption should not affect the simulation adversely because the charge time to reach equilibrium is very less than the spacecraft spin rate.

A. Particle traces

In order to estimate the effect of the spatially variable spacecraft sheath, a particle trajectory simulation was constructed. Particles were launched from the instrument aperture and propagated through the electric field until they exit the domain (130 m diameter × 34 m height cylinder). Particles were flown in the reverse direction (away from the aperture) because the vast majority of particles launched from the edge of the domain would not be detected at the aperture location.

The python SCIPY ordinary differential equation (ODE) function was used to integrate the particle position and velocity, using the "lsoda" integrator.[33,34] This integrator was chosen because it can adaptively switch between integration techniques based on the local stiffness of the current integration step. Integration steps were performed manually for two primary reasons:

1. The equations of motion are based in time; however, the integration is based on the distance when the particle exits the domain. This means that it is difficult to pass an exact time range to the integrator. Rather, it is easier to manually continue integration steps until the particle crosses the domain boundary and then breaks the integration routine.
2. For each individual step of the integration from point-to-point, python controls the internal timestep of the integration. When choosing how far to place the next integration point, however, an adaptive timestep was calculated based on the local acceleration due to the electric field and particle velocity. This is opposed to passing a predetermined set of time points into the routine for a complete end to end integration. A typical particle trace was composed of ∼10 000 points.

The integration was not performed with a predetermined set of timesteps fed to the integrator, but rather each integration point was evaluated to determine the next integration time step. This evaluation of the time step, dt, was based on the instantaneous particle velocity, $\vec{v}$, and acceleration, $\vec{a}$, as

$$dt = \frac{C}{|\vec{a}||\vec{v}|}, \tag{2}$$

where C is a constant chosen such that the particles typically exited the domain in about 10 000 steps. Electric field, $\vec{E}$, is the primary force mechanism and reaches several volts per meter near the booms. Because the magnetic field can vary quickly in time and it would be impractical to parameterize over all possibilities, the magnetic field was ignored for this case study. This approach is justified due to the gyroradius being much larger than the simulation domain (∼1 km for a 10 eV electron in a 10 nT field). This approach is further validated by the consistency in time of the bias (Fig. 1), indicating that the changing magnetic field vector does not play a significant role. The equation of motion to be integrated is therefore

$$m d\vec{v} = -q\vec{E}dt. \tag{3}$$

Note the negative sign on the right hand side; this is applied to computationally integrate the particle paths backward from the aperture to the domain boundary. For the final simulation run, four million particles were flown per species (electrons/ions), one million from each instrument. The trajectories were randomly distributed over a unit sphere (90° in azimuth per instrument) with logarithmic energy sampling from 10 eV to 30 keV. The energy range corresponds to the energy range of FPI upon launch.

The overall process for the simulation is as follows:

1. Load background potential data (as calculated in the SPIS model).
2. Take the gradient to obtain the electric field.
3. Sample n particles from a predefined logarithmic energy/spherical angle distribution.
4. For each particle:
   (a) placed at the center of instrument aperture (each instrument's individual aperture location was used);
   (b) while in the simulation domain (±17 m along the spin axis, 65 m radius in the spin plane):
      i. calculate acceptable time, t', to the next integration point based on local field strength and particle velocity and
      ii. use lsoda to integrate the particle position and velocity up to t';
   (c) remove particles from the domain.
5. Record all data to the file.

The initial and final position and velocity vectors are recorded to a data file. The error in the angle between the two velocities is calculated by the law of cosines.

IV. RESULTS AND FLIGHT VALIDATION

Particles were binned into 32 uniformly spaced azimuthal bins, 16 uniformly spaced elevation bins, and 32 logarithmically space energy bins. These bins were chosen to match the FPI measurement space. For each bin, a detection bias, η_d, was measured by comparing expected particles counted, c_e, and actual detected particles counted, c_a, per bin,

$$\eta_d = \frac{c_a}{c_e}. \tag{4}$$

An angle-angle plot of detection bias, η_d, for the lowest energy bin (10–13 eV) is shown in Fig. 4. As expected, the electron map is largely an inverse of the ion map due to the opposite polarity. Both electrons and ions show a nonuniform detection bias, with some areas reaching a ±60% bias.

In the extreme cases, the green filled pixels in the ion data represent areas where the simulated instrument is "blind." What this means is that it was not possible for a low energy particle originating in that look direction to reach the instrument aperture. This makes intuitive sense as these look directions are directly along the extended booms, and so any particle originating from this area would have an electric field applied over a long distance. This is not to say that these pixels

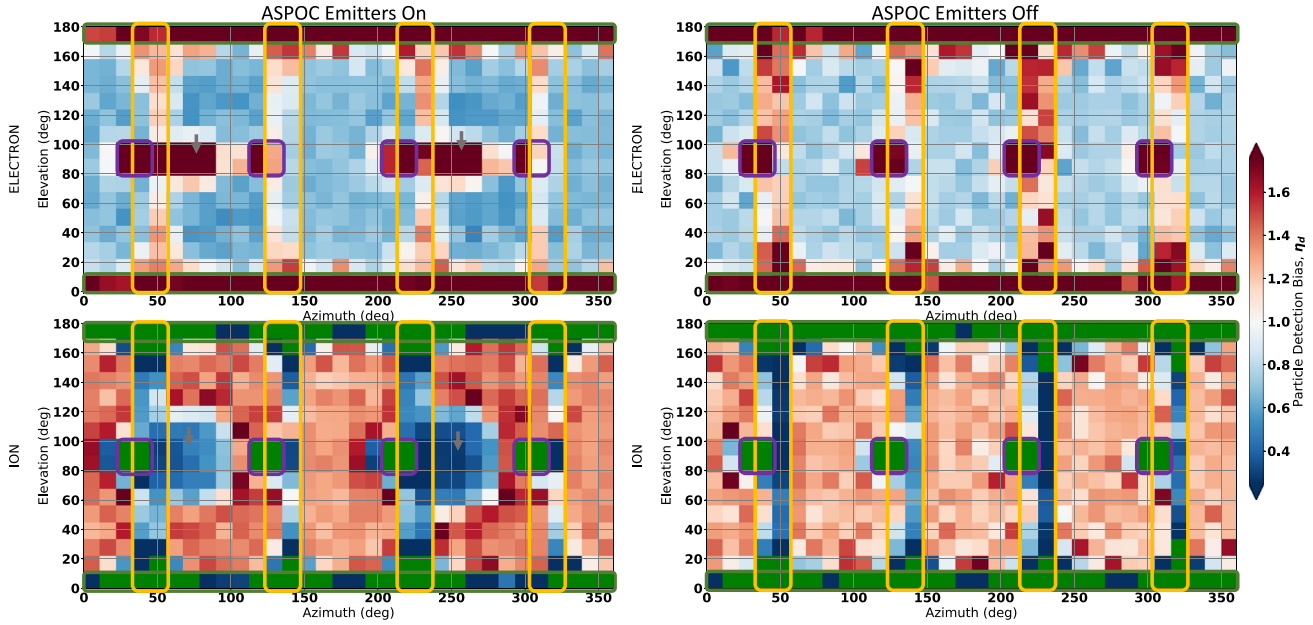

FIG. 4. Detection bias map for electrons (top) and ions (bottom) for the lowest FPI energy range (∼10–13 eV). The left pair is a simulation with the ASPOC emitters active, introducing a detection bias from the indium ion plume, and the right pair has the emission plume removed. Red areas represent a region of overcounting, and blue areas represent the areas of undercounting. Colored rectangles indicate areas of qualitative agreement among the spacecraft (Fig. 2), and gray arrows indicate areas influenced by the ASPOC plume. Green pixels in the ions indicate areas where no simulated particles could be detected.

will never collect counts, however, as particles may still be steered into these look directions by the electric field. Rather, it is to say that no particle detected in any pixel will have originated from the green look directions (at the lowest energies).

Several areas of localized bias are annotated in a similar fashion to the flight maps in Fig. 2:

1. The green rectangles outlining the top and bottom horizontal bands are caused by charging of the ADP boom, along the spacecraft spin axis (Fig. 3). The FPI angular bins are not uniform in coverage but rather overlap significantly near the poles.[2] Because of this, the angular separation between the azimuthal bins for the highest and lowest elevations is small. This means that all particles in the upper and lower elevation bins are essentially traveling along the line of the ADP boom. They are therefore in the strongest part of the electric field shown in Fig. 3 for an extended period of time and suffer significant deflection. Both the flight data and simulation data show a bias from the ADP; however, the simulation shows a more uniform effect in azimuth, whereas the flight data are more ragged. This is because the ADP is a wire lattice structure, which is difficult to accurately model with a surface mesh in a simulated environment.
2. The purple squares are caused by the SDP wire booms, located at 30°, 120°, 210°, and 300° in the spin plane (90° elevation). The 2 × 2 pixel squares represent the look directions which are right down the line of the boom, similar to the effect in item 1. All spacecraft, in all times examined, also show this effect; however, the magnitude tends to vary in the flight data. For example, in Fig. 2, the purple boxes outline a clear increase in bias, but the increase is not consistent among all the purple boxes. This may be simple quantization; the azimuthal bins are 11.25° wide and the wire booms do not necessarily lie cleanly within a single bin or on a boundary.
3. The yellow rectangle bias is also caused by the SDPs. As seen in Fig. 3, the potential from the SDPs extends several meters radially away from the wire boom. Similar to item 2, this effect is present in the flight data but is not totally uniform between cases. This is consistent with the nature of the potential at position 1 in Fig. 3.

These three regions match well with the flight electron data shown in Fig. 2. The gray arrows in Fig. 4 annotate the expected location of the ASPOC emission plume (≈80° and 260°) and associate the space charge effect in the particle bias. Some of the gray + annotations in Fig. 2 may be associated with the ASPOC plumes (gray arrow locations); however, the gray + sign regions were generally not reproduced in the simulation. Because the flight data are not consistent across the four observatories and the ASPOC signature did not match the expectation from the simulation, it was chosen to use the ASPOC-off simulation case for further investigation.

While the primary regions of bias in the flight data are reproduced by the simulation, the absolute magnitude of the bias is larger in the simulation to a varying degree over time and observatory. Due to the complexity of surface impact detection, the trajectory simulation does not account for particles absorbed by the spacecraft (notably the booms), which may lead to the simulation over-counting in these areas, leading to a perceived increase in detection bias. The simulation also does not model collisional effects, recombination, or neutralization of the ambient plasma, which may lead to an exaggeration of the electric field.

While it was not possible to find similarly clean, low energy ion data to use as a validation over the entire sky, it is possible to confirm that some "green pixel" locations do represent near blind areas to the DIS units. Figure 5 shows a cold ion beam detected in December of

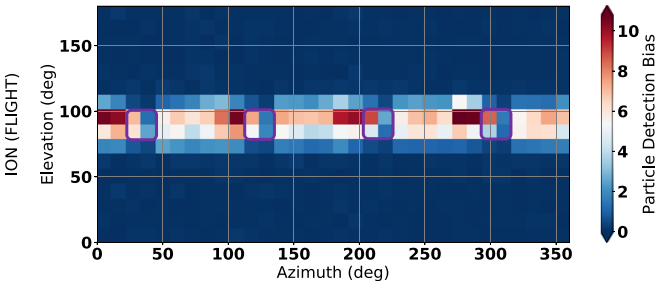

FIG. 5. Detection bias map (~10–13 eV) for DIS flight data from MMS3 on December 28, 2016. A narrow ion beam which swept around the spacecraft as it spun was dramatically reduced in intensity when coming from the look direction of the SDP wire booms. Purple squares represent the approximate look direction of the SDP.

2016.[27] The ion beam had a peak energy near the spacecraft potential, meaning that the ions made it through the spacecraft potential sheath but were low enough in energy to be deflected away from the SDP wire booms. This resulted in the counts being reduced in the direction of the SDP at the lowest energy bin. This is evidenced by the reduced detection bias in the approximate SDP locations, inside the purple squares. Note that because this was a cold ion beam in the belly band of the spacecraft, in an otherwise low density plasma, it is not possible to evaluate the effect of the ADP boom in a similar manner to these data.

Figure 6 shows a full bias map for the entire energy range. Green pixels are, as in previous figures, indications of where the simulation could not detect particles originating from a given look direction/energy combination. The vertical dimension represents 32 stacked sequences of 0°–180° in elevation, with energy increasing toward the top of the plot. This are, essentially, 32 stacked angle-angle plots, such as shown in Fig. 4, one per energy bin. This format is consistent with an FPI energy/angle skymap.[2] As such, the horizontal striping that is seen is representative of changes over elevation, whereas the gradual fading of the color, vertically, is representative of changes over energy. While the bias does falloff with energy, there are still areas of high bias (>20%) even upwards of 1000 eV. Some of the green colored, blind, look directions are also present up to several hundreds of electron volts. These areas tend to be the areas associated with looking down the length of the SDP booms. This makes sense as the SDP booms are 60 m long, thus affecting the local environment over a large distance. This is compounded with the fact that, while FPI looks at the entire sky, the actual aperture is fairly small (a few square centimeters), meaning that a particle deflected a small amount in some directions may miss detection altogether. This is noteworthy, as this effect could help to explain spin tones[26] in the high energy data. This result is consistent with that found on Cluster,[35] where the wire booms are one of the primary drivers of electrostatic steering effects.

V. CHARACTERIZATION OF TRAJECTORY ERROR

Figure 7 shows a statistical distribution of trajectory error vs energy. A Gaussian fit to each energy bin yields a line for peak error (red) and Gaussian full width at half max (FWHM, blue). In this distribution, at 1000 eV, there are no particles with greater than a one degree error in the angle. What this implies is that, while the particles near the SDP boom may have been pushed to a different detection bin (Fig. 6), they were not pushed very far in an absolute sense. The distribution of angular error with respect to energy shows a consistent, predictable behavior with a maximum error of ~30° at 10 eV.

The error distribution is quite wide for a given energy, meaning that the error in the angle is highly dependent on the exact trajectory. More precise descriptions of error can be made on the basis of energy and look direction. Figure 8 shows a distribution of detected particle error per elevation and azimuthal bin. A particle at (0, 0) would therefore have no associated error and be detected with the correct trajectory. All bays show a bimodal distribution with a depression in counting around an elevation of 0. This is consistent with the effect of the SDP booms shown in Fig. 4. There is also some asymmetry in the azimuthal direction, particularly in the ions which is likely due to the fact that the SDP booms are not on FPI bay boundaries and therefore have an asymmetric effect on the FPI bay. Note that this figure is collapsed over energy, not limited to the lowest energy bin. This means that most of the particles (higher energies) have lower associated error, thus the peak of the distribution around (0, 0).

The trajectory error can be used to calculate a mean error, or uncertainty, in the look direction of a given particle. This is shown in Fig. 9. Here, the user of the data can be given a measure of confidence in the count rates at various locations of the FPI skymap. As expected, the uncertainty is increased near the SDP wire booms (periodic signature in azimuth, decreasing in energy) and the ADP lattice booms (horizontal striping, decreasing in energy). The energy at which the error is generally less than one 11.25° measurement bin is around 50 eV.

Overall, the simulation paints an interesting picture: while MMS had a prelaunch requirement for no more than a single volt of potential between any two points on its surface throughout flight,[2] the absolute spacecraft potential combined with the long booms and emitted plumes results in an asymmetric and nonuniform distribution of collected particles.

VI. APPLICATION

By binning the particles based on (1) which direction they were observed to be from at the aperture and (2) which direction they originated from at the domain boundary, a mapping can be generated for where any detected particle came from. Figure 10 shows a similar top panel as in Fig. 4 for electrons (left) and ions (right). Each colored dot, and the corresponding outlined pixel, indicates a chosen look direction which is examined in the middle and bottom panels. The middle panel shows where a particle detected at the colored dot could have originated at infinity (the domain boundary). The bottom panel indicates the converse; if a particle originates from the colored direction, this is the area where the particle may be detected.

Looking at each of these regions in some detail:

Orange is placed in a look direction above one of the SDPs in elevation. For the electrons, the bottom panel shows that particles originating from this look direction tended to travel down and to the right before they were detected. The center panel shows that particles that were detected from this look direction tended to originate from either side, with some coming from a higher elevation. These behaviors are consistent with the SDP having a positive charge and attracting electrons toward it. The ions show a complementary behavior, with the SDP repelling particles. The bottom panel shows particles originating from this look direction being pushed to the left, away from the SDP.

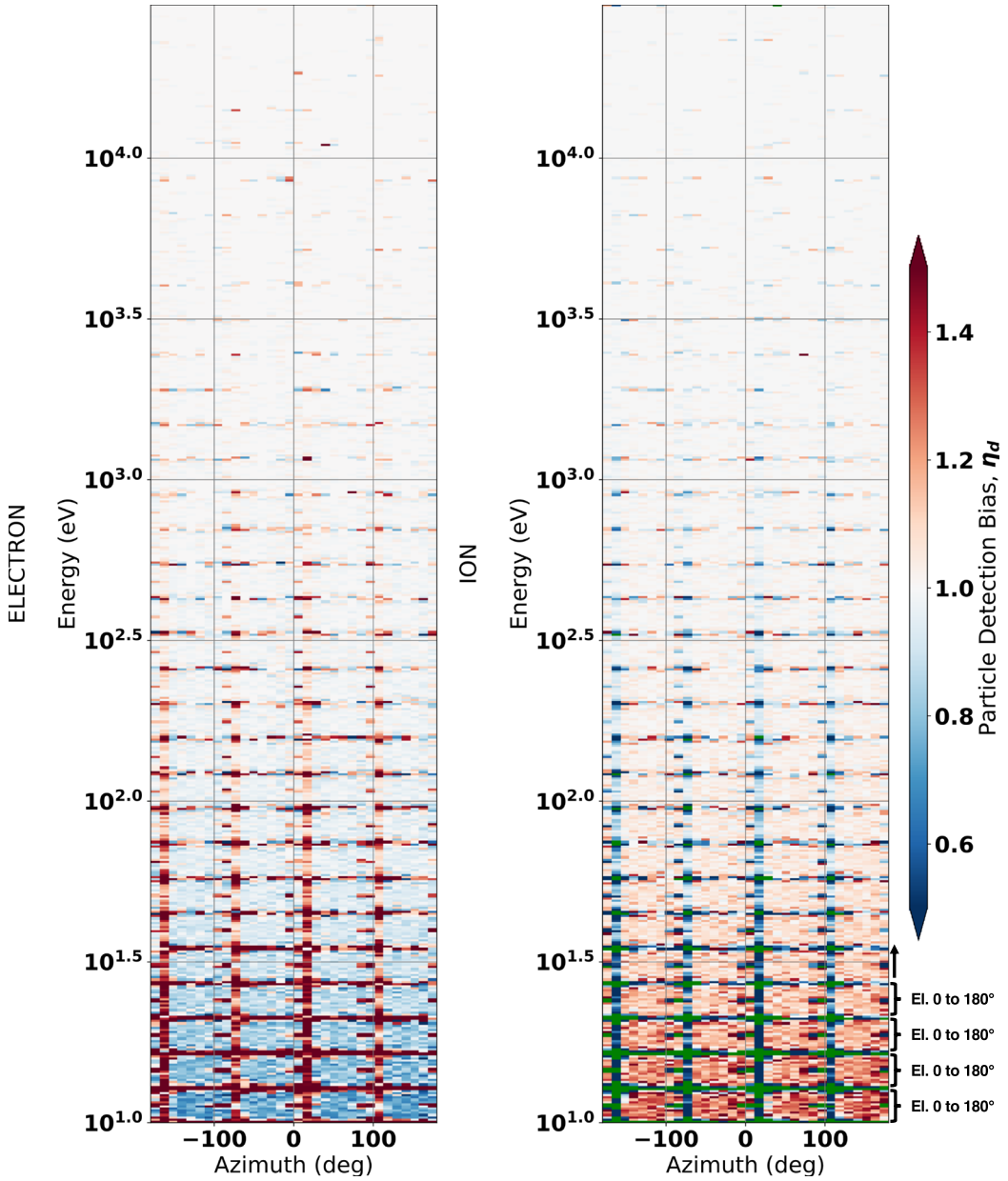

FIG. 6. Detection efficiency map corresponding to an FPI energy/angle sky map for electrons (left) and ions (right). Green coloring denotes areas where no detected particles originated in the simulation domain.

The center panel shows some particles detected from this look direction coming from lower elevations and greater azimuth. Note in the case of the ions that only about 50% of the particles were labeled correctly, but the overall bias of the point is near 1.0. This means that the particles which were lost were balanced out by gaining others. The electrons, by contrast, attracted more than that were lost, resulting in a net positive bias, shown in the top panel.

Gray is placed about two bins (22.5°) from the SDP boom. Here, the electrons are shown being pulled toward the boom, a net movement to the left, and the ions are shown being pushed away, a net movement to the right. The electrons show a net deficit in counts as the ions show a net surplus.

Bright green is placed right next to the SDP, about 11.25° offset from looking down its length. In both the ions and electrons, the target look direction is not the dominant pixel in any of the cases. The electrons show that less than 20% of the particles detected here actually came from this direction, and less than 20% of the particles that came from this direction were detected here. The ions are slightly better, at

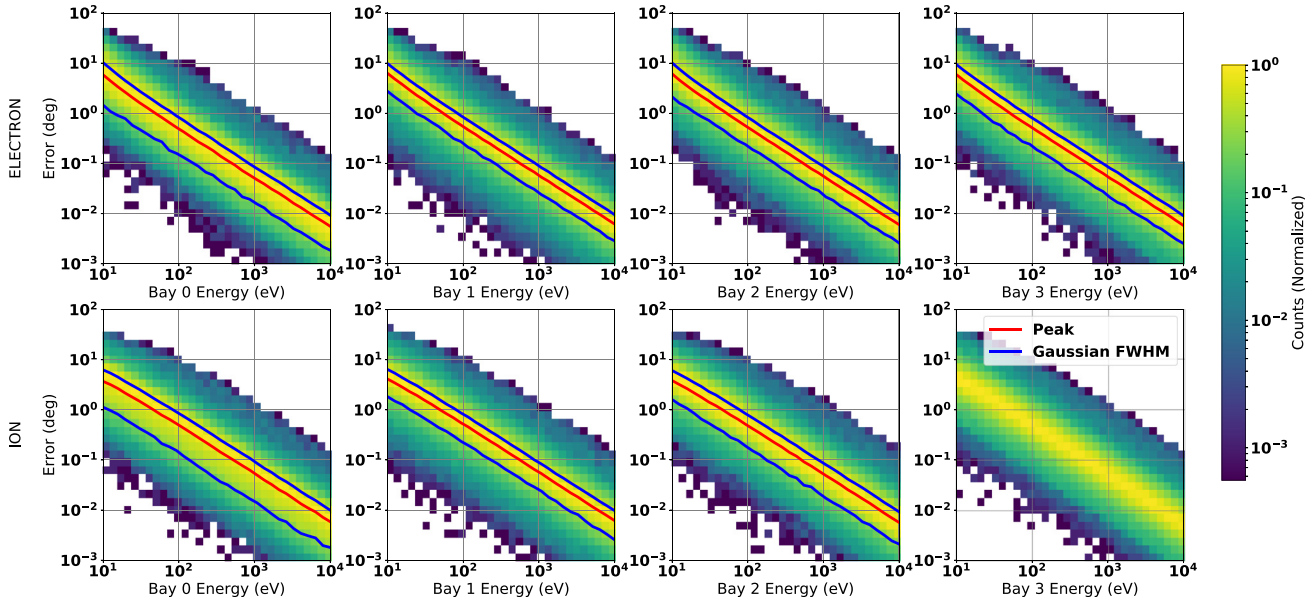

FIG. 7. Absolute error in the trajectory angle as a function of energy, separated per bay. The red line is a fit based to a Gaussian peak. The blue line is the width of the Gaussian peak associated with the red fit. Energy bins are approximately equal to the FPI measurement space.

around 30% for each. What is also noteworthy here is that some of the electrons traveled several bins from their initial trajectories. The ions, due to their higher mass ratio, did not travel quite as far but did migrate up to two bins.

Dark green is placed right on the SDP, looking roughly down its length. The electrons show particles mixing together from several nearby bins, matching the high uncertainty in this region (Fig. 9). This look direction represents one of the green colored blind look directions for the ions, however. The bottom panel indicates that all particles detected here originated from elsewhere, and the center panel indicates that no particles that originated from this look direction were detected using the instrument. This helps illustrate the effect of the ion beam periodically disappearing in Fig. 5.

Pink is placed looking up at the ADP boom. The ion effect is similar to the dark green case in that no particles actually originated from this direction were detected, and all particles detected here actually

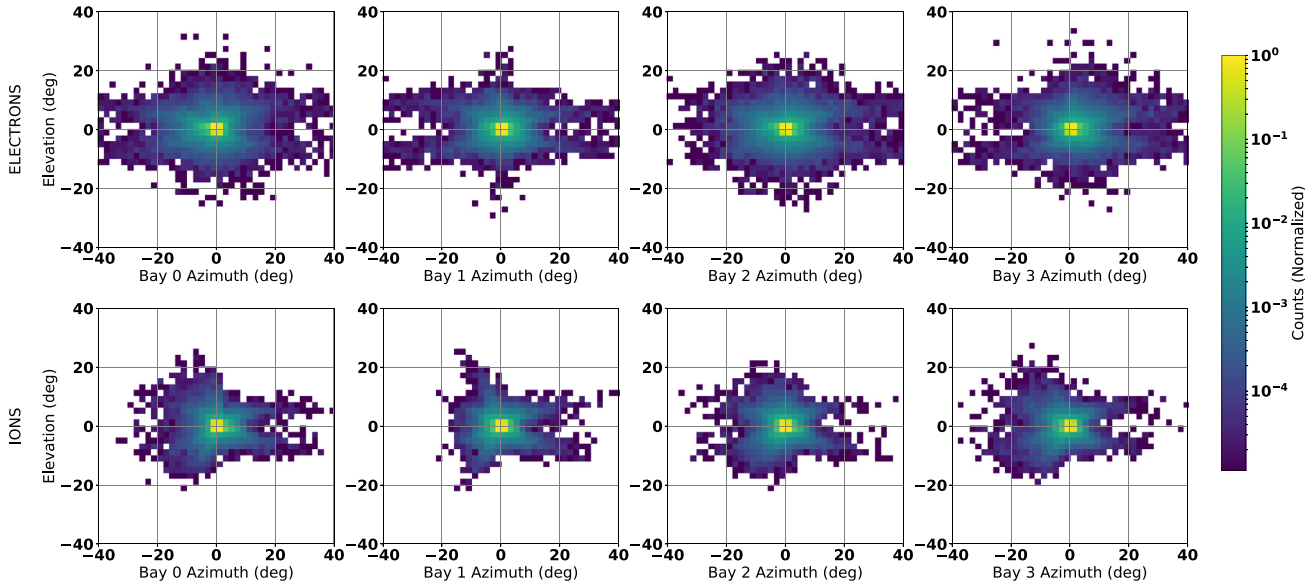

FIG. 8. Distributions of detected particles per bay, collapsed over all energies. Note that the ASPOC plumes are located in bays 0 and 2 and the SDP booms lie at 0 elevation.

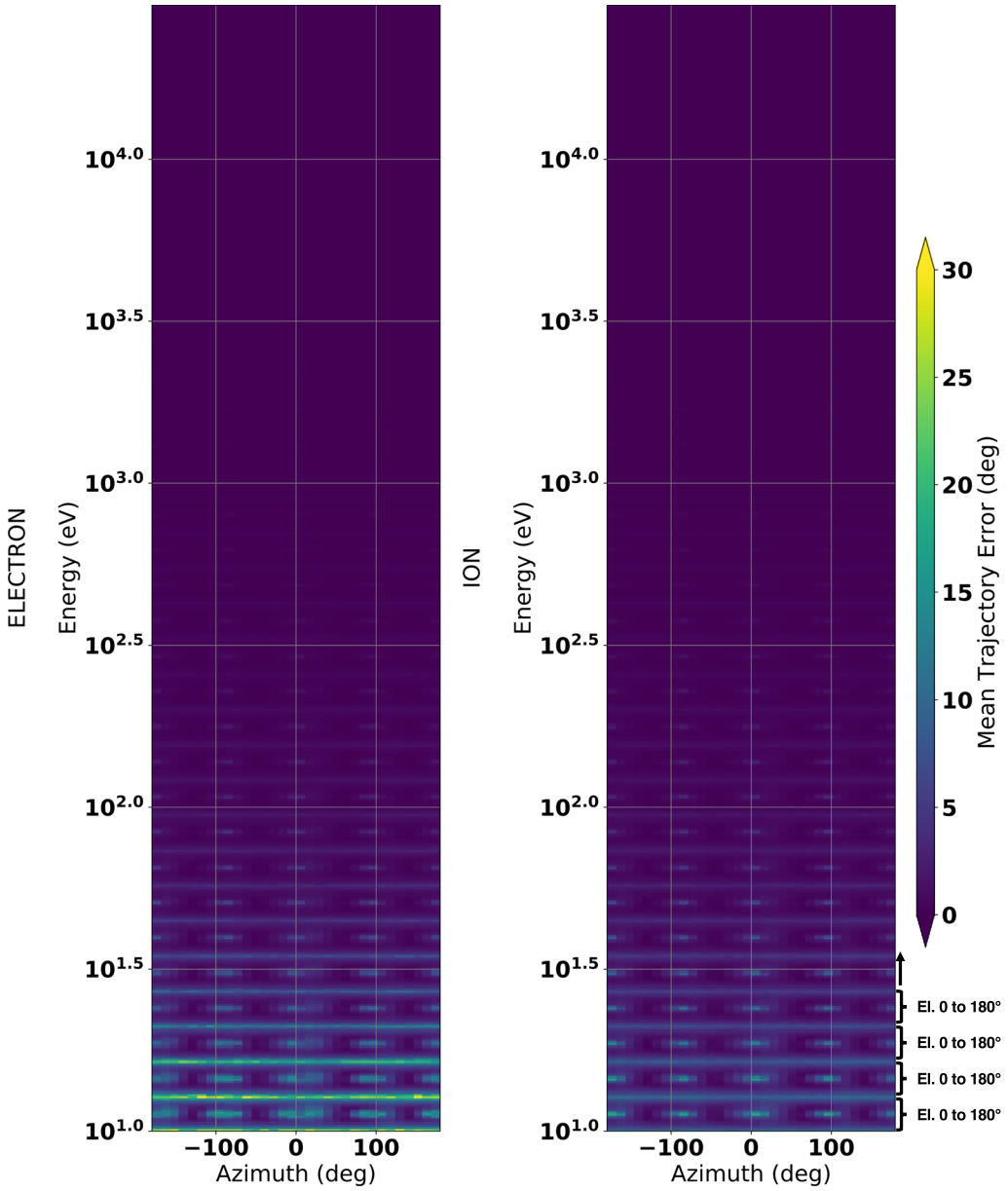

FIG. 9. Mean error in the look direction, or uncertainty, for a typical electron (left) and ion (right) FPI skymap. Higher uncertainty is evidenced around the extended booms.

came from lower elevations. The electrons have a large rectangular "area of influence"; however, this does not actually imply an error of potentially hundreds of degrees. Rather, this illustrates the issues with a rectilinear mapping of a spherical measurement space. There is a significant overlap of the polar pixels as they all look roughly in the same direction, and so while the spread of particles may be several bins wide, the error is actually not high as in terms of absolute angular separation, as shown in Figs. 7 and 8.

Combining this type of data for all pixels, a gradient map was developed showing count migration, shown in Fig. 11. Each look direction is represented by a single vector, which represents where counts should be repositioned to be in the correct bin, based on their trajectory at infinity. The color is proportional to the fraction of counts that need to be moved, and the vector, $\vec{V}$, length, and direction show the direction of movement, calculated as

$$\vec{V} = \left(\frac{C_R - C_L}{C_0}, \frac{C_U - C_D}{C_0}\right), \tag{5}$$

where C_0 represents the total counts detected in this pixel and C_R, C_L, C_U, and C_D are the counts originating from this direction that traveled right, left, up, or down in the image, respectively, before being

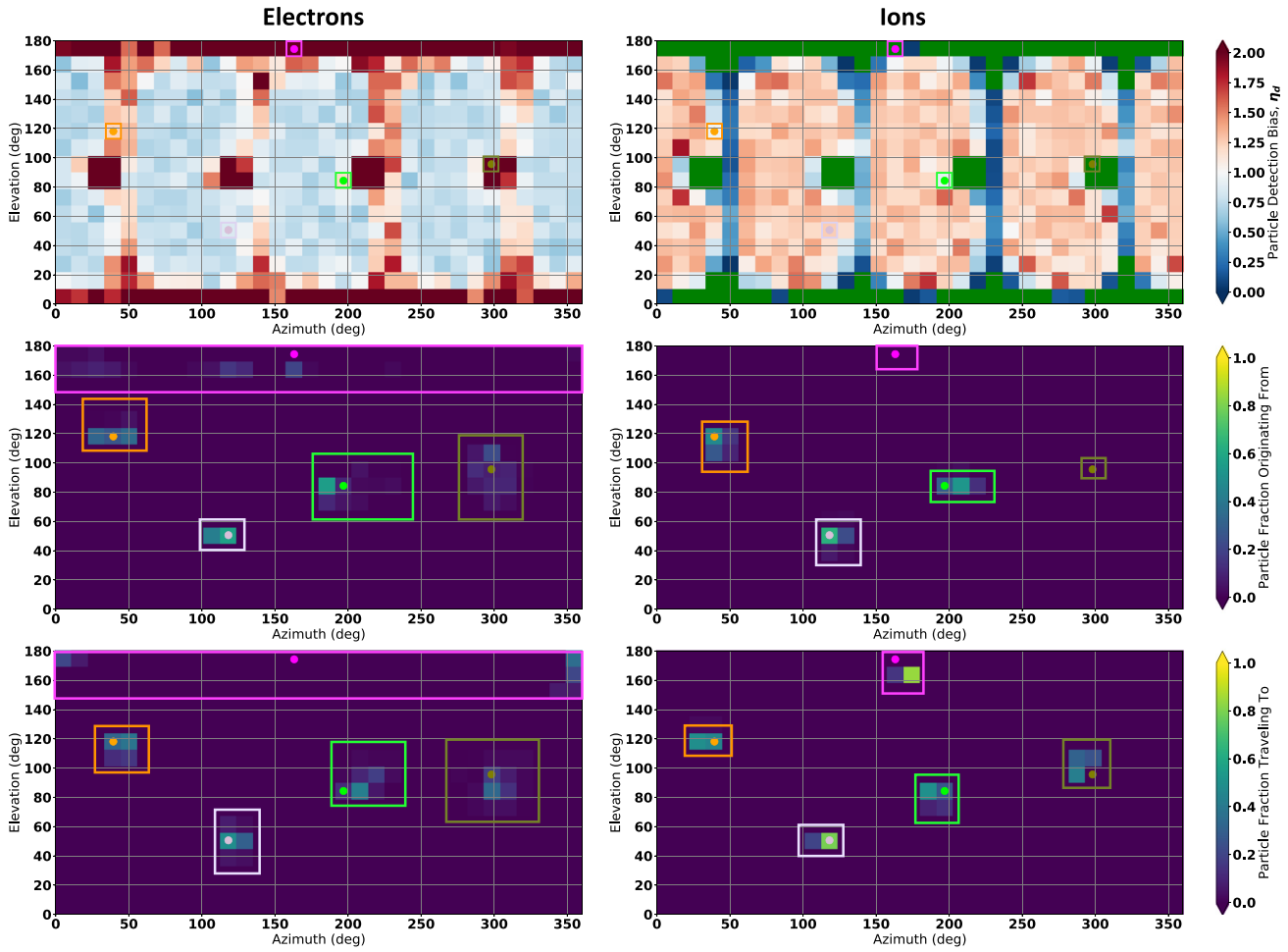

FIG. 10. Indications of where, for a given look direction (colored dots), a particle with that look direction at infinity is detected (bottom) and where a particle detected from that look direction originated at infinity (middle), for electrons (left) and ions (right). Colored outlines indicate the approximate area of influence for the matching colored look direction. The bias maps (∼10–13 eV) are the same as in Fig. 4.

detected. A vector that is short, but yellow, would therefore indicate that a large fraction of the particles should be repositioned, in a roughly Gaussian manner around the pixel of interest. Conversely, a long blue arrow would indicate that relatively few particles should be moved, but those that are moved go strongly in one direction.

VII. CONCLUSION

Spacecraft potential changes are accommodated by the ambient plasma forming a sheath around the spacecraft with a varying electric field that eventually decays. This sheath alters the trajectory of incoming particles as they move through the electric field. Characterizing this effect has been difficult due to the evolving nature of the sheath around a spinning spacecraft, with complex geometry, moving through a changing plasma, and the fact that high resolution angular data (in the spacecraft frame) have not been available. FPI, however, has the ability to resolve the effects of the plasma sheath in flight, due to the large number of analyzers placed around the spacecraft. Presented here is a method whereby the spacecraft plasma sheath was characterized using observed flight data and modeled using commercial software.[32] A numerical integration scheme was then used to trace particles from a broad distribution through the sheath, resulting in a bias map describing areas of enhanced or depressed counting statistics. The simulation was able to be validated in accordance with the observed flight measurements. The validated model was then used to characterize the movement of particles through the plasma sheath surrounding the spacecraft.

This analysis shows deflection of incoming particles, not only in energy but also significant deviations in the direction. Lower energy particles were deflected up to 45°, while particles up to 100 eV were deflected at least one detection bin (11.25°). Dropouts in the signal of cold ion beams seen in flight data,[27] were also explained as local areas of phase space that are blind to FPI due to the influence of the long wire booms on-board MMS.

Finally, maps of particle redistribution within a skymap were generated, as well as maps of uncertainty in the angular trajectory as a function of position in phase space. This characterization of particle

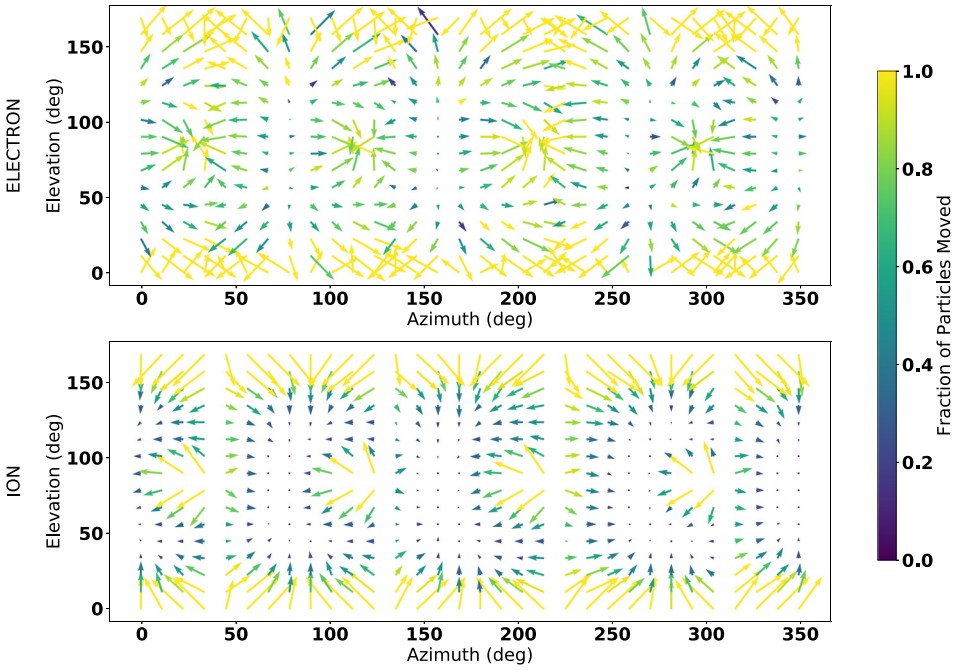

FIG. 11. Count migration gradient maps, for the lowest energy bin, showing the fraction of counts that should be moved (color) and the approximate location they should be moved to.

paths through the plasma sheath, and ensuing error when detected, will help to inform scientists when to evaluate signals from FPI, particularly at low energies or in the direction of the booms.

ACKNOWLEDGMENTS

This work was funded by NASA and the MMS mission. All source data are available from the MMS Science Data Center (https://lasp.colorado.edu/mms/sdc/public) Simulations of the MMS charging environment were conducted and provided by the European Space Agency.

REFERENCES

[1]J. Burch, T. Moore, R. Torbert, and B. Giles, "Magnetospheric multiscale overview and science objectives," Space Sci. Rev. **199**, 5–21 (2016).
[2]C. Pollock, T. Moore, A. Jacques, J. Burch, U. Gliese, Y. Saito, T. Omoto, L. Avanov, A. Barrie, V. Coffey *et al.*, "Fast plasma investigation for magnetospheric multiscale," Space Sci. Rev. **199**, 331–406 (2016).
[3]C. Carlson, D. Curtis, G. Paschmann, and W. Michel, "An instrument for rapidly measuring plasma distribution functions with high resolution," Adv. Space Res. **2**, 67–70 (1982).
[4]E. E. Scime, J. L. Phillips, and S. J. Bame, "Effects of spacecraft potential on three-dimensional electron measurements in the solar wind," J. Geophys. Res. **99**, 14769–14776, https://doi.org/10.1029/94JA00489 (1994).
[5]L. Parker and E. Whipple, "Theory of spacecraft sheath structure, potential, and velocity effects on ion measurements by traps and mass spectrometers," J. Geophys. Res. **75**, 4720–4733, https://doi.org/10.1029/JA075i025p04720 (1970).
[6]H. B. Garrett, "The charging of spacecraft surfaces," Rev. Geophys. **19**, 577–616, https://doi.org/10.1029/RG019i004p00577 (1981).
[7]A. C. Rager *et al.*, "Electron crescent distributions as a manifestation of diamagnetic drift in an electron scale current sheet: Magnetospheric multiscale observations using new 7.5 ms fast plasma investigation moments," Geophys. Res. Lett. **45**(2), 578–584, https://doi.org/10.1002/2017GL076260 (2018).
[8]D. J. Gershman, J. C. Dorelli, A. F. Viñas, and C. J. Pollock, "The calculation of moment uncertainties from velocity distribution functions with random errors," J. Geophys. Res. **120**, 6633–6645, https://doi.org/10.1002/2014JA020775 (2015).
[9]K. Torkar, R. Nakamura, M. Tajmar, C. Scharlemann, H. Jeszenszky, G. Laky, G. Fremuth, C. Escoubet, and K. Svenes, "Active spacecraft potential control investigation," Space Sci. Rev. **199**, 515–544 (2016).
[10]R. Torbert, H. Vaith, M. Granoff, M. Widholm, J. Gaidos, B. Briggs, I. Dors, M. Chutter, J. Macri, M. Argall *et al.*, "The electron drift instrument for MMS," Space Sci. Rev. **199**, 283–305 (2016).
[11]R. Torbert, C. Russell, W. Magnes, R. Ergun, P.-A. Lindqvist, O. LeContel, H. Vaith, J. Macri, S. Myers, D. Rau *et al.*, "The fields instrument suite on MMS: Scientific objectives, measurements, and data products," Space Sci. Rev. **199**, 105–135 (2016).
[12]D. J. Gershman, L. A. Avanov, S. A. Boardsen, J. C. Dorelli, U. Gliese, A. C. Barrie, C. Schiff, W. R. Paterson, R. B. Torbert, B. L. Giles *et al.*, "Spacecraft and instrument photoelectrons measured by the dual electron spectrometers on MMS," J. Geophys. Res. **122**, 11548–11558, https://doi.org/10.1002/2017JA024518 (2017).
[13]Y. Miyake, C. Cully, H. Usui, and H. Nakashima, "Plasma particle simulations of wake formation behind a spacecraft with thin wire booms," J. Geophys. Res. **118**, 5681–5694, https://doi.org/10.1002/jgra.50543 (2013).
[14]P.-A. Lindqvist, G. Olsson, R. Torbert, B. King, M. Granoff, D. Rau, G. Needell, S. Turco, I. Dors, P. Beckman *et al.*, "The spin-plane double probe electric field instrument for MMS," Space Sci. Rev. **199**, 137–165 (2016).
[15]H. Zhao, K. Torkar, R. Schmidt, W. Riedler, and C. Escoubet, "The influence of the photosheath on the very low energy electrons during active potential control," Adv. Space Res. **21**, 745–748 (1998).
[16]R. Ergun, D. Malaspina, S. Bale, J. McFadden, D. Larson, F. Mozer, N. Meyer-Vernet, M. Maksimovic, P. Kellogg, and J. Wygant, "Spacecraft charging and ion wake formation in the near-sun environment," Phys. Plasmas **17**, 072903 (2010).
[17]B. Thiébault, A. Hilgers, E. Sasot, H. Laakso, P. Escoubet, V. Génot, and J. Forest, "Potential barrier in the electrostatic sheath around a magnetospheric spacecraft," J. Geophys. Res. **109**, A12207, https://doi.org/10.1029/2004JA010398 (2004).
[18]S. Guillemant, V. Génot, J.-C. M. Velez, P. Sarrailh, A. Hilgers, and P. Louarn, "Simulation study of spacecraft electrostatic sheath changes with the heliocentric distances from 0.044 to 1 au," IEEE Trans. Plasma Sci. **41**, 3338–3348 (2013).

[19]R. Marchand and P. A. R. Lira, "Kinetic simulation of spacecraft–environment interaction," IEEE Trans. Plasma Sci. **45**, 535–554 (2017).
[20]X. Wang, J. Pilewskie, H.-W. Hsu, and M. Horányi, "Plasma potential in the sheaths of electron-emitting surfaces in space," Geophys. Res. Lett. **43**, 525–531, https://doi.org/10.1002/2015GL067175 (2016).
[21]A. Dove, M. Horanyi, X. Wang, M. Piquette, A. R. Poppe, and S. Robertson, "Experimental study of a photoelectron sheath," Phys. Plasmas **19**, 043502 (2012).
[22]H. Reme, J. Bosqued, J. Sauvaud, A. Cros, J. Dandouras, C. Aoustin, J. Bouyssou, T. Camus, J. Cuvilo, C. Martz *et al.*, "The cluster ion spectrometry (CIS) experiment," *The Cluster and Phoenix Missions* (Springer, 1997), pp. 303–350.
[23]J. Geach, S. Schwartz, V. Génot, O. Moullard, A. Lahiff, and A. Fazakerley, "A corrector for spacecraft calculated electron moments," Ann. Geophys. **23**, 931–943 (2005).
[24]J. McFadden, C. Carlson, D. Larson, J. Bonnell, F. Mozer, V. Angelopoulos, K.-H. Glassmeier, and U. Auster, "THEMIS ESA first science results and performance issues," *The THEMIS Mission* (Springer, 2009), pp. 477–508.
[25]R. Ergun, S. Tucker, J. Westfall, K. Goodrich, D. Malaspina, D. Summers, J. Wallace, M. Karlsson, J. Mack, N. Brennan *et al.*, "The axial double probe and fields signal processing for the MMS mission," Space Sci. Rev. **199**, 167–188 (2016).
[26]S. Toledo-Redondo, "In-situ detection of cold plasma in the earth's magnetosphere," Earth Space Sci. (to be published).
[27]D. Gershman, "Systematic uncertainties in plasma parameters reported by the fast plasma investigation on MMS," J. Geophys. Res. (to be published).
[28]D. Hastings and H. Garrett, *Spacecraft-Environment Interactions* (Cambridge University Press, 2004).
[29]M. A. Lieberman and A. J. Lichtenberg, *Principles of Plasma Discharges and Materials Processing* (John Wiley & Sons, 2005).
[30]F. Cipriani, C. Escoubet, K. Torkar, R. Nakamura, G. Déprez, D. Rodgers, and Y. Khotyaintsev, "Simulation of the electrostatic environment of the magnetospheric multiscale mission using the active spacecraft potential control system," in Proceedings of the 14th Spacecraft Charging Technology Conference (2016).
[31]F. Cipriani, C. Escoubet, K. Torkar, R. Nakamura, G. Déprez, D. Rodgers, Y. Khotyaintsev, and A. Barrie, "Simulated effects of aspocs on plasma measurements performed onboard the magnetospheric multiscale mission," in Proceedings of the 15th Spacecraft Charging Technology Conference (2018).
[32]J.-F. Roussel, F. Rogier, G. Dufour, J.-C. Mateo-Velez, J. Forest, A. Hilgers, D. Rodgers, L. Girard, and D. Payan, "SPIS open-source code: Methods, capabilities, achievements, and prospects," IEEE Trans. Plasma Sci. **36**, 2360–2368 (2008).
[33]L. Petzold and A. Hindmarsh, *LSODA: Computing and Mathematics Research Division* (Lawrence Livermore National Laboratory, Livermore, CA, 1997).
[34]T. E. Oliphant, "SCIPY: Open source scientific tools for python," Comput. Sci. Eng. **9**, 10–20 (2007).
[35]C. Cully, R. Ergun, and A. Eriksson, "Electrostatic structure around spacecraft in tenuous plasmas," J. Geophys. Res. **112**, A09211, https://doi.org/10.1029/2007JA012269 (2007).